# An isogeometric method for the Reissner-Mindlin plate bending problem

L. Beirão da Veiga[a], A. Buffa[b], C. Lovadina[c], M. Martinelli[c,1], G. Sangalli[c]

[a]*Dipartimento di Matematica "F. Enriques", Università degli Studi di Milano, Via Saldini 50, 20133 Milano, Italy*
[b]*IMATI - CNR, Via Ferrata 1, 27100 Pavia, Italy*
[c]*Dipartimento di Matematica "F. Casorati", Università di Pavia, Via Ferrata 1, 27100 Pavia, Italy*

**Abstract**

We present a new isogeometric method for the discretization of the Reissner-Mindlin plate bending problem. The proposed scheme follows a recent theoretical framework that makes possible to construct a space of smooth discrete deflections $W_h$ and a space of smooth discrete rotations $\mathbf{\Theta}_h$ such that the Kirchhoff contstraint is exactly satisfied at the limit. Therefore we obtain a formulation which is natural from the theoretical/mechanical viewpoint and locking free by construction. We prove that the method is uniformly stable and satisfies optimal convergence estimates. Finally, the theoretical results are fully supported by numerical tests.

*Keywords:* Isogeometric analysis, Reissner Mindlin plates, De Rham diagram

## 1. Introduction

The Reissner-Mindlin theory is widely used to describe the bending behavior of an elastic plate loaded by a transverse force. Despite its simple

*Email addresses:* lourenco.beirao@unimi.it (L. Beirão da Veiga), annalisa@imati.cnr.it (A. Buffa), carlo.lovadina@unipv.it (C. Lovadina), martinelli@imati.cnr.it (M. Martinelli), giancarlo.sangalli@unipv.it (G. Sangalli)
[1]Corresponding author

formulation, the discretization by means of finite elements is not straightforward, since standard low-order schemes exhibit a severe lack of convergence whenever the thickness is too small with respect to the other characteristic dimensions of the plate. This undesirable phenomenon, known as *shear locking*, is nowadays well understood: as the plate thickness tends to zero, the Reissner–Mindlin model enforces the Kirchhoff constraint, which is typically too severe for Finite Element Methods (FEM), especially if low-order polynomials are employed (see, for instance, the monograph by Brezzi and Fortin [1]). Roughly speaking, the root of the shear locking phenomenon is that *the space of discrete functions which satisfy the Kirchhoff constraint is very small, and does not properly approximate a generic plate solution.* The most popular way to overcome the shear locking phenomenon in FEM is to reduce the influence of the shear energy by considering a mixed formulation and/or suitable *shear reduction operator*. As a consequence, the choice of the discrete spaces requires particular care, also because of the possible occurrence of *spurious modes*. A vast engineering and mathematical literature is devoted to the design and analysis of plate elements for FEM; we mention here, in a totally non-exhaustive way, the works [2, 3, 4, 5, 6, 7, 8, 9, 10, 11, 12].

In 2005, IsoGeometric Analysis (IGA) has been introduced by T.J.R. Hughes and co-authors in [13] as a novel technique for the discretization of partial differential equations. IGA is having a growing impact on several fields, from fluid dynamics [14, 15], to structural mechanics [16, 17, 18, 19] and electromagnetics [20, 21]. A comprehensive reference for IGA is the book [22].

IGA methodologies are designed with the aim of improving the interoperability between numerical simulation of physical phenomena and the Computer Aided Design (CAD) systems. Indeed, the ultimate goal is to drastically reduce the error in the representation of the computational domain and the re-meshing by the use of the "exact" CAD geometry directly at the coarsest level of discretization. This is achieved by using B-Splines or Non Uniform Rational B-Splines (NURBS) for the geometry description as well as for the representation of the unknown fields. The use of Spline or NURBS functions, together with isoparametric concepts, results in an extremely successful idea and paves the way to many new numerical schemes enjoying features that would be extremely hard to achieve within a standard FEM. Splines and NURBS offer a flexible set of basis functions for which refinement, de-refinement, degree elevation and mesh deformation are very

efficient (e.g., [19]). Beside the fact that one can directly treat geometries described by Splines and NURBS parametrizations, these functions are interesting in themselves since they easily allow global smoothness beyond the classical $C^0$-continuity of FEM. This feature has been advantageously exploited in recent works, for example [17], and [23], and studied in [24], [25].

Furthermore, the intrinsic regularity of the Spline basis functions opened the way to completely new discretization schemes for Maxwell equations [20, 21], as well as for other problems, such as, the Stokes problem [15]. These schemes are based on suitable *smooth* approximation of differential forms, verifying a De Rham diagram in the spirit of [26]. The proposed theoretical framework can be usefully adopted also for discretizing the Reissner-Mindlin plate system which is the object of the present paper. Indeed, it makes possible to construct a space of smooth discrete deflections $W_h$ as discrete 0-forms and a space of smooth discrete rotations $\boldsymbol{\Theta}_h$ as discrete 1-forms such that it holds:

$$\nabla W_h \subseteq \boldsymbol{\Theta}_h.$$

This allows us to select approximation spaces containing a subspace which both exactly satisfies the Kirchhoff constraint and has optimal approximation features. Therefore, we obtain a simple formulation which is natural from the theoretical/mechanical viewpoint since it is built to be locking free, and it is easy to study.

Finally, the method inherits all the advantages, mentioned above, which are typical of IGA: the capability to incorporate exactly CAD geometries, and the flexibility in the choice of the polynomial degree and function regularity. Regarding the first advantage, the importance of reproducing the exact geometry in plate analysis has been underlined very clearly in [27].

The outline of the paper is the following. Section 2 is devoted to the description of Reissner-Mindlin model and 3 provides basics definition of spline spaces. Our discretization method is proposed in Section 4 and analysed in Section 5. Finally, Section 6 is devoted to the numerical validation.

## 2. The Reissner-Mindlin plate bending problem

Let $\Omega$ be a Lipschitz bounded open set of $\mathbb{R}^2$ representing the midsurface of the plate and let $\Gamma$ be its boundary. Other assumptions on the domain $\Omega$ will be set at the end of Section 3.2. We assume that the boundary $\Gamma$ is the

union of three disjoint sets

$$\overline{\Gamma} = \overline{\Gamma}_f \cup \overline{\Gamma}_s \cup \overline{\Gamma}_c \ ,$$

with $\Gamma_f, \Gamma_s, \Gamma_c$ being a finite union of connected components. The plate is clamped in $\Gamma_c$, simply supported in $\Gamma_s$ and free in $\Gamma_f$. We assume for simplicity of exposition that all boundary conditions are homogeneous, and that the union $\Gamma_s \cup \Gamma_c$ has positive measure, in order to neglect rigid body motions of the plate. Finally, let $\Gamma_s$ be divided into a soft and a hard part (both being a finite union of connected components), i.e. $\Gamma_s = \Gamma_{ss} \cup \Gamma_{sh}$. We then set the spaces for deflections and rotations

$$\begin{aligned} W_0 &= \{v \in H^1(\Omega) \ : \ v = 0 \text{ on } \ \Gamma_s \cup \Gamma_c\} \\ \boldsymbol{\Theta}_0 &= \{\boldsymbol{\eta} \in [H^1(\Omega)]^2 \ : \ \boldsymbol{\eta} = 0 \text{ on } \ \Gamma_c \ , \boldsymbol{\eta} \cdot \boldsymbol{t} = 0 \text{ on } \ \Gamma_{sh}\}, \end{aligned}$$

with $\boldsymbol{t}$ the unit tangent to $\Gamma$ obtained by an anti-clockwise rotation of the outward normal $\boldsymbol{n}$.

Following the Reissner-Mindlin model, see for instance [1], the plate bending problem requires to solve

$$\begin{cases} \text{Find } \boldsymbol{\theta} \in \boldsymbol{\Theta}_0, w \in W_0 \text{ such that} \\ a(\boldsymbol{\theta}, \boldsymbol{\eta}) + \mu k t^{-2} (\boldsymbol{\theta} - \nabla w, \boldsymbol{\eta} - \nabla v) = (f, v) \quad \forall \boldsymbol{\eta} \in \boldsymbol{\Theta}_0, v \in W_0 \ , \end{cases} \tag{1}$$

where $\mu$ is the shear modulus and $k$ is the so-called shear correction factor. Above, $t$ represents the plate thickness, $w$ the deflection, $\boldsymbol{\theta}$ the rotation of the normal fibers and $f$ the applied scaled transversal load. Moreover, $(\cdot, \cdot)$ stands for the standard scalar product in $L^2(\Omega)$ and the bilinear form $a(\cdot, \cdot)$ is defined by

$$a(\boldsymbol{\theta}, \boldsymbol{\eta}) = (\mathbb{C}\varepsilon(\boldsymbol{\theta}), \varepsilon(\boldsymbol{\eta})),$$

with $\mathbb{C}$ the positive definite tensor of bending moduli and $\varepsilon(\cdot)$ the symmetric gradient operator. Introducing the scaled shear stresses $\boldsymbol{\gamma} = \mu k t^{-2}(\boldsymbol{\theta} - \nabla w)$, Problem (1) can be written in terms of the following mixed variational formulation:

$$\begin{cases} \text{Find } \boldsymbol{\theta} \in \boldsymbol{\Theta}_0, w \in W_0, \boldsymbol{\gamma} \in \boldsymbol{\Sigma} \text{ such that} \\ a(\boldsymbol{\theta}, \boldsymbol{\eta}) + (\boldsymbol{\gamma}, \boldsymbol{\eta} - \nabla v) = (f, v) \quad \forall \boldsymbol{\eta} \in \boldsymbol{\Theta}_0, v \in W_0 \\ (\boldsymbol{\theta} - \nabla w, \boldsymbol{s}) - \dfrac{t^2}{\mu k} (\boldsymbol{\gamma}, \boldsymbol{s}) = 0 \quad \forall \boldsymbol{s} \in \boldsymbol{\Sigma} \ , \end{cases} \tag{2}$$

where $\mathbf{\Sigma} = [L^2(\Omega)]^2$.

The above problem is well posed and $t$-uniformly stable when using the $H^1$ norm for the spaces $\mathbf{\Theta}_0, W_0$, and the norm:

$$||\boldsymbol{s}||_{\mathbf{\Sigma}} := t\|\boldsymbol{s}\|_{L^2} + \sup_{(\boldsymbol{\eta},v)\in\mathbf{\Theta}_0\times W_0} \frac{(\boldsymbol{s}, \boldsymbol{\eta} - \nabla v)}{(||\boldsymbol{\eta}||^2_{H^1} + ||v||^2_{H^1})^{1/2}}.$$

for the space $\mathbf{\Sigma}$ (see [1], for instance). To simplify notation, and without any loss of generality, we will assume $\mu k = 1$ in the analysis that follows.

## 3. B-splines and piece-wise smooth functions

### *3.1. B-spline spaces and piece-wise smooth functions in one dimension*

Given positive integers $p$ and $n$, such that $n \geq p + 1$, we introduce the ordered knot vector

$$\Xi := \{0 = \xi_1, \xi_2, \ldots, \xi_{n+p+1} = 1\},$$

where we allow repetitions of knots, that is, we assume $\xi_1 \leq \xi_2 \leq \cdots \leq \xi_{n+p+1}$. In the following we will only work with *open* knot vectors, which means that the first $p + 1$ knots in $\Xi$ are equal to 0, and the last $p + 1$ are equal to 1, and we assume that all internal knots have multiplicity $r$, $1 \leq r \leq p + 1$, so that

$$\Xi = \{\underbrace{\zeta_1, \ldots, \zeta_1}_{p+1 \text{ times}}, \underbrace{\zeta_2, \ldots, \zeta_2}_{r \text{ times}}, \ldots, \underbrace{\zeta_m, \ldots, \zeta_m}_{p+1 \text{ times}}\}.$$

The vector

$$\mathcal{Z} = \{0 = \zeta_1, \zeta_2, \ldots, \zeta_m = 1\}$$

represents the (ordered) vector of knots without repetitions, and the relation $m = \frac{n-p-1}{r} + 2$ holds.

Through the iterative procedure detailed in [13] we construct $p$-degree (that is, $(p + 1)$-order) B-spline basis functions, denoted by $B_i$, for $i = 1, \ldots, n$. These basis functions are piecewise polynomials of degree $p$ on the subdivision $\{\zeta_1, \ldots, \zeta_m\}$. At $\zeta_i$ they have $\alpha := p - r$ continuous derivatives. Therefore, $-1 \leq \alpha \leq p - 1$: the maximum multiplicity allowed, $r = p + 1$, gives $\alpha = -1$, which stands for a discontinuity at each $\zeta_i$. Each basis function

$B_i$ is non-negative and supported in the interval $[\xi_i, \xi_{i+p+1}]$. Moreover, these B-spline functions constitute a partition of unity, that is

$$\sum_{i=1}^{n} B_i(x) = 1 \quad \forall x \in (0,1).$$

The space of B-splines spanned by the basis functions $B_i$ will be denoted by

$$S_\alpha^p := \text{span}\{B_i\}_{i=1}^n.$$

Derivatives of splines are splines as well. Let $S_{\alpha+1}^{p+1}$ and $S_\alpha^p$ be spline spaces constructed, according with the notation above, on the same subdivision $\{\zeta_1, \ldots, \zeta_m\}$. Then, it is easy to see that

$$\left\{ \frac{d}{dx} v : v \in S_{\alpha+1}^{p+1} \right\} = S_\alpha^p, \tag{3}$$

Notice moreover that

$$\# S_\alpha^p = p + 1 + (m-2)(p-\alpha), \tag{4}$$

and

$$\# S_{\alpha+1}^{p+1} = p + 2 + (m-2)(p-\alpha), \tag{5}$$

where # is used to denote the dimension of the linear space. Then, from (4)–(5), $\# S_{\alpha+1}^{p+1} = \# S_\alpha^p + 1$, in agreement with the fact that the derivative is a surjective operator from $S_{\alpha+1}^{p+1}$ to $S_\alpha^p$ and has a one-dimensional kernel, the constants.

We denote by $\mathcal{C}_\alpha^\infty$ the space of piecewise smooth functions on $(0,1)$, whose restriction to each subinterval $(\zeta_i, \zeta_{i+1})$ admits a $C^\infty$ extension to the closed interval $[\zeta_i, \zeta_{i+1}]$ with $\alpha$ continuous derivatives at $\zeta_i$, for all $i = 2, \ldots, m-1$.

*3.2. B-spline spaces and piece-wise smooth functions in two dimensions*

The definition of B-splines spaces given above can be extended to two dimensions as follows. Let us consider the square $\widehat{\Omega} = (0,1)^2 \subset \mathbb{R}^2$, which will be referred to as *parametric domain*. Given integers $p_d$, $r_d$, $n_d$ and $\alpha_d = p_d - r_d$, with $d = 1, 2$, we introduce the knot vectors $\Xi_d = \{\xi_{1,d}, \xi_{2,d}, \ldots, \xi_{n_d+p_d+1,d}\}$ and the associated vectors $\mathcal{Z}_d = \{\zeta_{1,d}, \ldots, \zeta_{m_d,d}\}$ as in the one-dimensional case. Associated with these knot vectors there is a *mesh* $\widehat{\Omega}_h$ of the parametric domain, that is, a partition of $(0,1)^2$ into rectangles:

$$\widehat{\Omega}_h = \{Q = \otimes_{d=1,2}(\zeta_{i_d,d}, \zeta_{i_d+1,d}),\ 1 \le i_d \le m_d - 1\}. \tag{6}$$

Given an element $Q \in \widehat{\Omega}_h$, we set $h_Q = \mathrm{diam}(Q)$, and define the global mesh size $h = \max\{h_Q,\ Q \in \widehat{\Omega}_h\}$.

In this paper we make the following assumption:

**Assumption 3.1.** *The parametric mesh $\widehat{\Omega}_h$ is shape regular.*

It is important to remark that, due to the tensor product structure, **shape regularity implies quasi-uniformity**, i.e., there exists a positive constant $\mathsf{k}$, fixed once and for all, such that

$$\mathsf{k}h \leq h_Q \leq h\ , \quad \forall Q \in \widehat{\Omega}_h. \tag{7}$$

We associate to the two given knot vectors $\Xi_d$, $d = 1, 2$ the $p_d$-degree univariate B-splines basis functions $B_{i,d}$, with $i = 1, \ldots, n_d$. Then, on the associated mesh $\widehat{\Omega}_h$, we define the tensor-product B-spline basis functions as

$$B_{ij} := B_{i,1} \otimes B_{j,2}, \quad i = 1, \ldots, n_1,\ j = 1, \ldots, n_2\,.$$

Then, the tensor product B-spline space is defined as the space spanned by these basis functions, namely

$$S^{p_1,p_2}_{\alpha_1,\alpha_2} \equiv S^{p_1,p_2}_{\alpha_1,\alpha_2}(\widehat{\Omega}_h) := S^{p_1}_{\alpha_1} \otimes S^{p_2}_{\alpha_2} = \mathrm{span}\{B_{ij}\}_{i=1,j=1}^{n_1,n_2}\,.$$

Notice that the space $S^{p_1,p_2}_{\alpha_1,\alpha_2}(\widehat{\Omega}_h)$ is fully characterized by the mesh $\widehat{\Omega}_h$, by $p_1$, $p_2$, $\alpha_1$ and $\alpha_2$, as our notation reflects. The minimum regularity of the space is $\alpha := \min\{\alpha_d :\ d = 1, 2\}$.

In a similar way, we define on $\widehat{\Omega}_h$ the space of piecewise smooth functions with interelement regularity on the vertical and horizontal mesh edges given by $\alpha_1$ and $\alpha_2$ respectively. This is denoted by

$$\mathcal{C}^{\infty}_{\alpha_1,\alpha_2} = \mathcal{C}^{\infty}_{\alpha_1,\alpha_2}(\widehat{\Omega}_h) = \mathcal{C}^{\infty}_{\alpha_1} \otimes \mathcal{C}^{\infty}_{\alpha_2}.$$

Precisely, a function in $\mathcal{C}^{\infty}_{\alpha_1,\alpha_2}$ admits a $C^{\infty}$ extension in the closure of each element $Q \in \widehat{\Omega}_h$, has $\alpha_1$ continuous derivatives on the edges $\{(x_1, x_2) : x_1 = \zeta_{i,1}, \zeta_{j,2} < x_2 < \zeta_{j+1,2}\}$, for $j = 1, \ldots, m_2 - 1$, $i = 2, \ldots, m_1 - 1$ and $\alpha_2$ continuous derivatives on the edges $\{(x_1, x_2) : \zeta_{j,1} < x_1 < \zeta_{j+1,1}, x_2 = \zeta_{i,2}, \}$, for $j = 1, \ldots, m_1 - 1$, $i = 2, \ldots, m_2 - 1$. From the definitions, $S^{p_1,p_2}_{\alpha_1,\alpha_2} \subset \mathcal{C}^{\infty}_{\alpha_1,\alpha_2}$.

From an initial coarse mesh $\widehat{\Omega}_{h_0}$, refinements are constructed by knot insertion (with possible repetition, see [28]). Therefore, we end up considering

a family of meshes $\{\widehat{\Omega}_h\}_{h\leq h_0}$ and associated spaces, with the global mesh size $h$ playing the role of family index, as usual in finite element literature.

We assume that our computational domain $\Omega \subset \mathbb{R}^2$ can be exactly parametrized by a geometrical mapping $\mathbf{F} : \widehat{\Omega} \longrightarrow \Omega$ which belongs to $(\mathcal{C}^{\infty}_{\alpha_1,\alpha_2}(\widehat{\Omega}_h))^2$, with piecewise smooth inverse, and is independent of the mesh family index $h$. The geometrical map $\mathbf{F}$ naturally induces a mesh $\Omega_h$ on $\Omega$, which is the image of (6). Notice that, as a conseguence of (7) and the boundness of $\mathbf{F}$ and its inverse, there exist two positive constants $\mathsf{k}'$, $\mathsf{k}''$, fixed once and for all, such that

$$\mathsf{k}'h \leq h_K \leq \mathsf{k}''h \qquad \forall K \in \Omega_h \ . \tag{8}$$

Finally , $\widehat{\Gamma}_f$, $\widehat{\Gamma}_s$ $\widehat{\Gamma}_c \subset \widehat{\Gamma} = \partial\widehat{\Omega}$ denote the preimage of $\Gamma_f$ $\Gamma_s$ and $\Gamma_c$, respectively.

## 4. Discretization of the scalar and vector fields

*4.1. Spline spaces on the parametric domain*

Given the two (horizontal and vertical) knot vectors, $\mathcal{Z}_1 = \{\zeta_{1,1}, \ldots, \zeta_{m_1,1}\}$ and $\mathcal{Z}_2 = \{\zeta_{1,2}, \ldots, \zeta_{m_2,2}\}$, and the associated mesh $\widehat{\Omega}_h$ on the parametric domain $\widehat{\Omega}$, with $1 \leq \alpha \leq p+1$, we introduce the following spaces:

$$\widehat{W}_h = S^{p,p}_{\alpha,\alpha}(\widehat{\Omega}_h) \tag{9a}$$

$$\widehat{\boldsymbol{\Theta}}_h = S^{p-1,p}_{\alpha-1,\alpha}(\widehat{\Omega}_h) \times S^{p,p-1}_{\alpha,\alpha-1}(\widehat{\Omega}_h) \tag{9b}$$

$$\widehat{\boldsymbol{\Sigma}}_h = \nabla\widehat{W}_h + \widehat{\boldsymbol{\Theta}}_h \tag{9c}$$

Since by construction $\nabla\widehat{W}_h \subseteq \widehat{\boldsymbol{\Theta}}_h$, it clearly holds that $\widehat{\boldsymbol{\Sigma}}_h = \widehat{\boldsymbol{\Theta}}_h$.

Essential boundary conditions has to be set directly in the function spaces and this brings us to the definition:

$$\widehat{W}_{h,0} \equiv \widehat{W}_{h,0}(p,\alpha) = \left\{ v \in S^{p,p}_{\alpha,\alpha}(\widehat{\Omega}_h) \ : \ v = 0 \text{ on } \widehat{\Gamma}_s \cup \widehat{\Gamma}_c \right\} \tag{10a}$$

$$\widehat{\boldsymbol{\Theta}}_{h,0} \equiv \widehat{\boldsymbol{\Theta}}_{h,0}(p,\alpha) = \left\{ \boldsymbol{\eta} \in S^{p-1,p}_{\alpha-1,\alpha}(\widehat{\Omega}_h) \times S^{p,p-1}_{\alpha,\alpha-1}(\widehat{\Omega}_h) \ : \ \boldsymbol{\eta} = \mathbf{0} \text{ on } \widehat{\Gamma}_c \text{ and } \boldsymbol{\eta}\cdot\hat{\boldsymbol{t}} = 0 \text{ on } \widehat{\Gamma}_{sh} \right\} \tag{10b}$$

$$\widehat{\boldsymbol{\Sigma}}_{h,0} \equiv \widehat{\boldsymbol{\Sigma}}_{h,0}(p,\alpha) = \nabla\widehat{W}_{h,0} + \widehat{\boldsymbol{\Theta}}_{h,0} \tag{10c}$$

where $\hat{\boldsymbol{t}}$ is a unit tangent vector at $\widehat{\Gamma}_{sh}$. Notice that now $\nabla\widehat{W}_{h,0} \subseteq \widehat{\boldsymbol{\Theta}}_{h,0}$ only if $\widehat{\Gamma}_c = \emptyset$ and $\widehat{\Gamma}_{ss} = \emptyset$ (see e.g., [20]). As a conseguence, $\widehat{\boldsymbol{\Sigma}}_{h,0}$ needs a characterization which is the object of the next Lemma:

**Lemma 4.1.** *The following characterization holds*

$$\boldsymbol{s} \in \widehat{\boldsymbol{\Sigma}}_{h,0} \Leftrightarrow \begin{cases} \boldsymbol{s} \in \ \widehat{\boldsymbol{\Theta}}_h \\ \boldsymbol{s} \cdot \boldsymbol{t} = 0 \ \textit{on} \ \widehat{\Gamma}_{sh} \cup \widehat{\Gamma}_c \\ \boldsymbol{s}(\widehat{\boldsymbol{x}}) = \boldsymbol{0}, \ \textit{for every corner} \ \widehat{\boldsymbol{x}} \in \partial\widehat{\Omega} \ \textit{such that} \ \widehat{\boldsymbol{x}} \in \overline{\widehat{\Gamma}}_{ss} \cap \overline{\widehat{\Gamma}}_c. \end{cases} \tag{11}$$

*Moreover, given* $\boldsymbol{s} \in \widehat{\boldsymbol{\Sigma}}_{h,0}$*, there are* $v \in \widehat{W}_{h,0}$*,* $\boldsymbol{\eta} \in \widehat{\boldsymbol{\Theta}}_{h,0}$*, such that*

$$\begin{aligned} \boldsymbol{\eta} - \nabla v &= \boldsymbol{s}, \\ \|\boldsymbol{\eta}\|_{H^1(\widehat{\Omega})} + \|v\|_{H^1(\widehat{\Omega})} &\leq C h^{-1} \|\boldsymbol{s}\|_{L^2(\widehat{\Omega})}. \end{aligned} \tag{12}$$

*Proof.* Denote $\widetilde{\boldsymbol{\Sigma}}_{h,0}$ the space of fields that fulfill the characterization on the right hand side of (11). Let $\widehat{\boldsymbol{\Sigma}}_{h,0} \ni \boldsymbol{s} = \boldsymbol{\eta}^{\boldsymbol{s}} - \nabla v^{\boldsymbol{s}}$. Then, from (3), we easily see that $\nabla v^{\boldsymbol{s}}$ belongs to $S^{p-1,p}_{\alpha-1,\alpha}(\widehat{\Omega}_h) \times S^{p,p-1}_{\alpha,\alpha-1}(\widehat{\Omega}_h)$, and the boundary conditions that define (10a)–(10c) implies that $\boldsymbol{\eta}^{\boldsymbol{s}} - \nabla v^{\boldsymbol{s}}$ fulfills the homogeneous boundary conditions stated in (11). Thus $\widehat{\boldsymbol{\Sigma}}_{h,0} \subseteq \widetilde{\boldsymbol{\Sigma}}_{h,0}$.

In order to prove the inclusion $\widehat{\boldsymbol{\Sigma}}_{h,0} \supseteq \widetilde{\boldsymbol{\Sigma}}_{h,0}$, notice that the fields in $\widetilde{\boldsymbol{\Sigma}}_{h,0}$ which vanish on $\widehat{\Gamma}_c$ belong to $\widehat{\boldsymbol{\Theta}}_{h,0}$, therefore we need to show that the B-spline basis functions of $\widetilde{\boldsymbol{\Sigma}}_{h,0}$ whose support intersect $\widehat{\Gamma}_c$ belong to $\nabla\widehat{W}_{h,0}$. This is again easily seen from the structure of the spaces.

Let again $\widehat{\boldsymbol{\Sigma}}_{h,0} \ni \boldsymbol{s} = \boldsymbol{\eta}^{\boldsymbol{s}} - \nabla v^{\boldsymbol{s}}$. Define $v \in \widehat{W}_{h,0}$ such that

$$\frac{\partial v}{\partial \boldsymbol{n}} = -\boldsymbol{s} \cdot \boldsymbol{n} \text{ on } \widehat{\Gamma}_c \tag{13}$$

and such that the B-spline coefficients of $v$ not involved in (13) are set to zero. Because of the locality of the B-spline basis functions, $v$ is supported in a strip of element associated with the $p+1$ knot spans around $\widehat{\Gamma}_c$. By construction, the norm of $v$ is bounded by the norm of (13), then, by a scaling argument and inverse estimate,

$$\begin{aligned} \|\nabla v\|_{L^2(\widehat{\Omega})} &\leq C h^{1/2} \left\| \frac{\partial v}{\partial \boldsymbol{n}} \right\|_{L^2(\widehat{\Gamma}_c)} \\ &= C h^{1/2} \|\boldsymbol{s} \cdot \boldsymbol{n}\|_{L^2(\widehat{\Gamma}_c)} \\ &\leq C \|\boldsymbol{s}\|_{L^2(\widehat{\Omega})}. \end{aligned} \tag{14}$$

Since $\boldsymbol{s} + \nabla v$ vanishes on $\widehat{\Gamma}_c$, we can set

$$\boldsymbol{\eta} = \boldsymbol{s} + \nabla v \in \widehat{\boldsymbol{\Theta}}_{h,0},$$

and, using again an inverse estimate and (14), the following estimate holds

$$\begin{aligned}\|\boldsymbol{\eta}\|_{H^1(\widehat{\Omega})} &\leq Ch^{-1}\|\boldsymbol{\eta}\|_{L^2(\widehat{\Omega})} \\ &= Ch^{-1}\left(\|\boldsymbol{s}\|_{L^2(\widehat{\Omega})} + \|\nabla v\|_{L^2(\widehat{\Omega})}\right) \\ &\leq Ch^{-1}\|\boldsymbol{s}\|_{L^2(\widehat{\Omega})}.\end{aligned} \tag{15}$$

The property (12) follows from (14) and (15). □

*4.2. Spline spaces on the physical domain*

Once the finite dimensional spaces $\widehat{W}_{h,0}$, $\widehat{\boldsymbol{\Theta}}_{h,0}$ and $\widehat{\boldsymbol{\Sigma}}_{h,0}$ on the parametric domain $\widehat{\Omega}$ have been defined, we construct the corresponding spaces $W_{h,0}$, $\boldsymbol{\Theta}_{h,0}$ and $\boldsymbol{\Sigma}_{h,0}$ in the physical domain $\Omega$.

The deflections space $W_{h,0}$ is mapped from the reference domain via the geometrical parametrization $\mathbf{F} : \widehat{\Omega} \longrightarrow \Omega$, that is

$$W_{h,0} = \{\hat{v} \circ \mathbf{F}^{-1} : \hat{v} \in \widehat{W}_{h,0}(p,\alpha)\}.$$

For the rotations and shears spaces we use the covariant map:

$$\begin{aligned}\boldsymbol{\Theta}_{h,0} &= \left\{D\,\mathbf{F}^{-T}\,\hat{\mathbf{v}} \circ \mathbf{F}^{-1} : \hat{\mathbf{v}} \in \widehat{\boldsymbol{\Theta}}_{h,0}\right\}, \\ \boldsymbol{\Sigma}_{h,0} &= \left\{D\,\mathbf{F}^{-T}\,\hat{\mathbf{v}} \circ \mathbf{F}^{-1} : \hat{\mathbf{v}} \in \widehat{\boldsymbol{\Sigma}}_{h,0}\right\},\end{aligned}$$

where $D\,\mathbf{F}^{-T} = (D\,\mathbf{F}^{-1})^T$ is the transpose of the gradient of the inverse of the geometrical map $\mathbf{F}$. The push-forward by the covariant map has two main properties: *i)* it preserves the nullity of tangential components, *ii)* it maps gradient to gradients, i.e., by the chain rule, we have $\nabla w = D\,\mathbf{F}^{-T}\widehat{\nabla}\hat{w} \circ \mathbf{F}^{-1}$ when $w = \hat{w} \circ \mathbf{F}^{-1}$. Thus, we have that $\mathbf{v} \cdot \boldsymbol{t} = 0$ on $\Gamma_{sh}$ for all $\mathbf{v} \in \boldsymbol{\Theta}_{h,0}$ and, recalling Lemma 4.1, the following holds:

**Lemma 4.2.** *We have*

$$\boldsymbol{\Sigma}_{h,0} = \nabla W_{h,0} + \boldsymbol{\Theta}_{h,0},$$

*and, for $\boldsymbol{s} \in \boldsymbol{\Sigma}_{h,0}$, there exist $v \in W_{h,0}$, $\boldsymbol{\eta} \in \boldsymbol{\Theta}_{h,0}$, such that*

$$\begin{aligned}\boldsymbol{\eta} - \nabla v &= \boldsymbol{s}, \\ \|\boldsymbol{\eta}\|_{H^1(\Omega)} + \|v\|_{H^1(\Omega)} &\leq Ch^{-1}\|\boldsymbol{s}\|_{L^2(\Omega)}.\end{aligned} \tag{16}$$

We now turn to approximation properties and we make use of the approximation results proved in [29] and adapted in [20] for vector fields under covariant transformation.

**Lemma 4.3.** *Let $1 \leq \alpha \leq p+1$, and let $\mathbf{F} \in (\mathcal{C}^{\infty}_{\alpha,\alpha}(\widehat{\Omega}_h))^2$. There exist projectors $\Pi_{W_{h,0}} : W_0 \to W_{h,0}$, $\Pi_{\boldsymbol{\Theta}_{h,0}} : \boldsymbol{\Theta}_0 \to \boldsymbol{\Theta}_{h,0}$ and $\Pi_{\boldsymbol{\Sigma}_{h,0}} : \boldsymbol{\Sigma} \to \boldsymbol{\Sigma}_{h,0}$ such that, for all $1 < s \leq p+1$*

$$\|v - \Pi_{W_{h,0}}(v)\|_{H^1(K)} \leq Ch^{s-1}|v|_{H^s(\tilde{K})}, \qquad \forall K \in \Omega_h, \forall v \in W_0 \cap H^s(\tilde{K}),$$

*for all $1 \leq s \leq p$*

$$\|\boldsymbol{\eta} - \Pi_{\boldsymbol{\Theta}_{h,0}}(\boldsymbol{\eta})\|_{H^1(K)} \leq Ch^{s-1}|\boldsymbol{\eta}|_{H^s(\tilde{K})}, \qquad \forall K \in \Omega_h, \forall \boldsymbol{\eta} \in \boldsymbol{\Theta}_0 \cap (H^s(\tilde{K}))^2$$

*for all $1 < s \leq p$*

$$\|\boldsymbol{s} - \Pi_{\boldsymbol{\Sigma}_{h,0}}(\boldsymbol{s})\|_{L^2(K)} \leq Ch^{s}|\boldsymbol{s}|_{H^s(\tilde{K})}, \qquad \forall K \in \Omega_h, \forall \boldsymbol{s} \in \boldsymbol{\Sigma}^s,$$

*where*

$$\boldsymbol{\Sigma}^s = (\boldsymbol{\Theta}_0 + \nabla W_0) \cap (H^s(\tilde{K}))^2.$$

*Proof.* The projector $\Pi_{W_{h,0}}$ can be chosen as the quasi-interpolant proposed in [29] and homogeneuous boundary condition are imposed by setting to zero che coefficient of all the basis functions which are non-zero on $\Gamma_c$ and $\Gamma_s$. The projector $\Pi_{\boldsymbol{\Theta}_{h,0}}$ is the one constructed in [20], with boundary condition set only on $\Gamma_c$ and $\Gamma_{sh}$; and $\Pi_{\boldsymbol{\Sigma}_{h,0}}$ is the same with the set of boundary condition corresponding to (11). □

**Remark 4.1.** *If $\Gamma_c = \emptyset$ and $\Gamma_{ss} = \emptyset$, then $\nabla W_{h,0} \subseteq \boldsymbol{\Theta}_{h,0} = \boldsymbol{\Sigma}_{h,0}$. In this case, we can choose as interpolation operators the commuting projectors that are constructed in [21]: i.e., there are projectors $P_{W_{h,0}}$ and $P_{\boldsymbol{\Theta}_{h,0}}$ such that*

$$P_{\boldsymbol{\Theta}_{h,0}} \nabla = \nabla P_{W_{h,0}}.$$

*We refer to [21, 20] for the details.*

*4.3. The discrete problem*

We can now introduce our proposed method. The Galerkin formulation for the approximation of Problem (1), reads

$$\begin{cases} \text{Find } (\boldsymbol{\theta}_h, w_h) \in \boldsymbol{\Theta}_{h,0} \times W_{h,0} \text{ such that} \\ a(\boldsymbol{\theta}_h, \boldsymbol{\eta}_h) + t^{-2}(\boldsymbol{\theta}_h - \nabla w_h, \boldsymbol{\eta}_h - \nabla v_h) = (f, v_h) \quad \forall (\boldsymbol{\eta}_h, v_h) \in \boldsymbol{\Theta}_{h,0} \times W_{h,0}; \end{cases} \tag{17}$$

this is the discrete problem which is solved in our isogeometric code. For the purpose of its stability and convergence analysis, we introduce the discrete shear stress

$$\boldsymbol{\gamma}_h = t^{-2}(\boldsymbol{\theta}_h - \nabla w_h) \in \boldsymbol{\Sigma}_{h,0},$$

and reformulate Problem (17) in the following mixed form (analogous to Problem (2)):

$$\begin{cases} \text{Find } \boldsymbol{\theta}_h w_h, \boldsymbol{\gamma}_h) \in \boldsymbol{\Theta}_{h,0} \times W_{h,0} \times \boldsymbol{\Sigma}_{h,0} \text{ such that} \\ a(\boldsymbol{\theta}_h, \boldsymbol{\eta}_h) + (\boldsymbol{\gamma}_h, \boldsymbol{\eta}_h - \nabla v_h) = (f, v_h) \quad \forall \boldsymbol{\eta}_h \in \boldsymbol{\Theta}_{h,0}, v_h \in W_{h,0} \\ (\boldsymbol{\theta}_h - \nabla w_h, \boldsymbol{s}_h) - t^2(\boldsymbol{\gamma}_h, \boldsymbol{s}_h) = 0 \quad \forall \boldsymbol{s}_h \in \boldsymbol{\Sigma}_{h,0} \ . \end{cases} \tag{18}$$

Introducing, for all $(\boldsymbol{\beta}, u, \boldsymbol{\tau})$ and $(\boldsymbol{\eta}, v, \boldsymbol{s})$ in $\boldsymbol{\Theta}_0 \times W_0 \times \boldsymbol{\Sigma}$, the symmetric bilinear form

$$\mathcal{B}(\boldsymbol{\beta}, u, \boldsymbol{\tau}; \boldsymbol{\eta}, v, \boldsymbol{s}) = a(\boldsymbol{\beta}, \boldsymbol{\eta}) + (\boldsymbol{\tau}, \boldsymbol{\eta} - \nabla v) + (\boldsymbol{\beta} - \nabla u, \boldsymbol{s}) - t^2(\boldsymbol{\tau}, \boldsymbol{s}), \tag{19}$$

the continuous and discrete problems can be also written as

$$\mathcal{B}(\boldsymbol{\theta}, w, \boldsymbol{\gamma}; \boldsymbol{\eta}, v, \boldsymbol{s}) = (f, v) \quad \forall (\boldsymbol{\eta}, v, \boldsymbol{s}) \in \boldsymbol{\Theta}_0 \times W_0 \times \boldsymbol{\Sigma} \ , \tag{20}$$

and

$$\mathcal{B}(\boldsymbol{\theta}_h, w_h, \boldsymbol{\gamma}_h; \boldsymbol{\eta}_h, v_h, \boldsymbol{s}_h) = (f, v_h) \quad \forall (\boldsymbol{\eta}_h, v_h, \boldsymbol{s}_h) \in \boldsymbol{\Theta}_{h,0} \times W_{h,0} \times \boldsymbol{\Sigma}_{h,0} \ . \tag{21}$$

Note that, differently from what happens with most finite element methods (e.g. the well-known MITC elements, cf. [30, 5]), if one considers the limit case $t = 0$ in formulation (18), the second equation gives exactly $\boldsymbol{\theta}_h = \nabla w_h$. Therefore, substituting such identity in the first equation of (18), one gets the problem

$$\begin{cases} \text{Find } w_h \in W_{h,0} \text{ such that} \\ a(\nabla w_h, \nabla v_h) = (f, v_h) \quad \forall v_h \in W_{h,0} \ , \end{cases}$$

i.e. the Kirchhoff plate bending problem.

## 5. Convergence analysis

In this section we investigate the convergence properties of the method proposed in Section 4.

Under the assumption $\Gamma_c = \Gamma_{ss} = 0$, we present in Section 5.1 an analysis based only upon coercivity. A similar approach is proposed by Duran and Libermann in [7], but things are straightforard in our case, thanks to the commuting projectors that are at our disposal (see Remark 4.1).

On the other hand, for general boundary conditions, we need a more delicate analysis which is the object of Section 5.2.

*5.1. Coercivity-based convergence analysis*

We assume in this section:

**Assumption 5.1.** *It holds* $\Gamma_c = \emptyset$ *and* $\Gamma_{ss} = \emptyset$.

We recall that, under the above assumption, as noted in Remark 4.1 the following properties hold

$$\boldsymbol{\Theta}_{h,0} = \boldsymbol{\Sigma}_{h,0} \ , \quad P_{\boldsymbol{\Theta}_{h,0}} \nabla = \nabla P_{W_{h,0}}.$$

The following lemma holds.

**Lemma 5.1.** *Let* $(\boldsymbol{\theta}, w)$ *be the solution of Problem* (1) *and* $(\boldsymbol{\theta}_h, w_h)$ *be the solution of Problem* (17). *Let the shears* $\boldsymbol{\gamma} = t^{-2}(\boldsymbol{\theta} - \nabla w)$ *and* $\boldsymbol{\gamma}_h = t^{-2}(\boldsymbol{\theta}_h - \nabla w_h)$. *Then for* $1 < s \leq p$ *it holds*

$$||\boldsymbol{\theta}-\boldsymbol{\theta}_h||_{H^1(\Omega)}+||w-w_h||_{H^1(\Omega)}+t||\boldsymbol{\gamma}-\boldsymbol{\gamma}_h||_{L^2(\Omega)} \leq Ch^{s-1}(||\boldsymbol{\theta}||_{H^s(\Omega)}+t||\boldsymbol{\gamma}||_{H^{s-1}(\Omega)}) \ , \tag{22}$$

*where the constant* $C$ *is independent of* $h, t$.

*Proof.* From (1) and (17), we obtain

$$a(\boldsymbol{\theta} - \boldsymbol{\theta}_h, \boldsymbol{\eta}_h) + (\boldsymbol{\gamma} - \boldsymbol{\gamma}_h, \boldsymbol{\eta}_h - \nabla v_h) = 0 \quad \forall \boldsymbol{\eta}_h \in \boldsymbol{\Theta}_h, v_h \in W_h.$$

Therefore, for every $(\boldsymbol{\theta}_I, w_I) \in \boldsymbol{\Theta}_{0,h} \times W_{0,h}$, and $\boldsymbol{\gamma}_I := t^{-2}(\boldsymbol{\theta}_I - \nabla w_I) \in \boldsymbol{\Sigma}_{0,h}$, we infer

$$\begin{aligned} a(\boldsymbol{\theta}_I - \boldsymbol{\theta}_h, \boldsymbol{\eta}_h) + (\boldsymbol{\gamma}_I - \boldsymbol{\gamma}_h, \boldsymbol{\eta}_h - \nabla v_h) &= a(\boldsymbol{\theta}_I - \boldsymbol{\theta}, \boldsymbol{\eta}_h) \\ &+ (\boldsymbol{\gamma}_I - \boldsymbol{\gamma}, \boldsymbol{\eta}_h - \nabla v_h) \qquad \forall \boldsymbol{\eta}_h \in \boldsymbol{\Theta}_h, v_h \in W_h. \end{aligned} \tag{23}$$

Choosing $\boldsymbol{\eta}_h = \boldsymbol{\theta}_I - \boldsymbol{\theta}_h$ and $v_h = w_I - w_h$, we get

$$t^2(\boldsymbol{\gamma}_I - \boldsymbol{\gamma}_h) = \boldsymbol{\eta}_h - \nabla v_h.$$

Therefore, from (23) we get

$$a(\boldsymbol{\theta}_I - \boldsymbol{\theta}_h, \boldsymbol{\theta}_I - \boldsymbol{\theta}_h) + t^2(\boldsymbol{\gamma}_I - \boldsymbol{\gamma}_h, \boldsymbol{\gamma}_I - \boldsymbol{\gamma}_h) = a(\boldsymbol{\theta}_I - \boldsymbol{\theta}, \boldsymbol{\theta}_I - \boldsymbol{\theta}_h) + t^2(\boldsymbol{\gamma}_I - \boldsymbol{\gamma}, \boldsymbol{\gamma}_I - \boldsymbol{\gamma}_h). \tag{24}$$

Using standard arguments, from (24) we obtain

$$||\boldsymbol{\theta}_I - \boldsymbol{\theta}_h||_{H^1(\Omega)} + t||\boldsymbol{\gamma}_I - \boldsymbol{\gamma}_h||_{L^2(\Omega)} \leq C(||\boldsymbol{\theta}_I - \boldsymbol{\theta}||_{H^1(\Omega)} + t||\boldsymbol{\gamma}_I - \boldsymbol{\gamma}||_{L^2(\Omega)}) \ .$$

We choose now $\boldsymbol{\theta}_I = P_{\boldsymbol{\Theta}_{h,0}}\boldsymbol{\theta}$ and $w_I = P_{W_{h,0}}w$, where $P_{\boldsymbol{\Theta}_{h,0}}$ and $P_{W_{h,0}}w$ are the interpolation operators introduced in Section 4.2. By the choice of $\boldsymbol{\gamma}_I$, we obtain:

$$\boldsymbol{\gamma}_I := t^{-2}(\boldsymbol{\theta}_I - \nabla w_I) = t^{-2}P_{\boldsymbol{\Theta}_{h,0}}(\boldsymbol{\theta} - \nabla w) = P_{\boldsymbol{\Theta}_{h,0}}\boldsymbol{\gamma}.$$

Therefore, also using Lemma 4.3, we have

$$t||\boldsymbol{\gamma}_I - \boldsymbol{\gamma}||_{L^2(\Omega)} = t||P_{\boldsymbol{\Theta}_{h,0}}\boldsymbol{\gamma} - \boldsymbol{\gamma}||_{L^2(\Omega)} \leq Ch^{s-1}t||\boldsymbol{\gamma}||_{H^{s-1}(\Omega)}. \tag{25}$$

Furthermore, again due to Lemma 4.3, it holds

$$||\boldsymbol{\theta}_I - \boldsymbol{\theta}||_{H^1(\Omega)} = ||P_{\boldsymbol{\Theta}_{h,0}}\boldsymbol{\theta} - \boldsymbol{\theta}||_{H^1(\Omega)} \leq Ch^{s-1}||\boldsymbol{\theta}||_{H^{s-1}(\Omega)}. \tag{26}$$

Using the triangle inequality and (25)-(26), from Lemma 5.1 we get

$$||\boldsymbol{\theta} - \boldsymbol{\theta}_h||_{H^1(\Omega)} + t||\boldsymbol{\gamma} - \boldsymbol{\gamma}_h||_{L^2(\Omega)} \leq Ch^{s-1}(||\boldsymbol{\theta}||_{H^s(\Omega)} + t||\boldsymbol{\gamma}||_{H^{s-1}(\Omega)}) \ . \tag{27}$$

To get the error estimate on the deflections, we simply notice that it holds

$$\nabla(w - w_h) = (\boldsymbol{\theta} - \boldsymbol{\theta}_h) - t^2(\boldsymbol{\gamma} - \boldsymbol{\gamma}_h). \tag{28}$$

Estimate (22) now easily follows from (27)-(28).

□

*5.2. Convergence in a discrete norm*

In this section we suppose that general boundary conditions are set and thus Assumption 5.1 does not hold. On the other hand, we remind that (8) holds true and this is crucial in the subsequent analysis.

We will make use of the following discrete norm [6]:

$$\begin{aligned} |||\boldsymbol{\eta}, v|||^2_{\boldsymbol{\Theta}} &= ||\boldsymbol{\eta}||^2_{H^1(\Omega)} + \sum_{K\in\Omega_h} \frac{1}{t^2+h_K^2}||\nabla v - \boldsymbol{\eta}||^2_{L^2(K)} \\ |||\boldsymbol{s}|||^2_{\boldsymbol{\Sigma}} &= t^2||\boldsymbol{s}||^2_{L^2(\Omega)} + \sum_{K\in\Omega_h} h_K^2||\boldsymbol{s}||^2_{L^2(K)} \\ |||\boldsymbol{\eta}, v, \boldsymbol{s}|||^2 &= |||\boldsymbol{\eta}, v|||^2_{\boldsymbol{\Theta}} + |||\boldsymbol{s}|||^2_{\boldsymbol{\Sigma}} \ , \end{aligned} \tag{29}$$

for all $\boldsymbol{\eta} \in \boldsymbol{\Theta}_0$, $v \in W_0$ and $\boldsymbol{s} \in \boldsymbol{\Sigma}$. It is easy to check that it holds

$$|||\boldsymbol{\eta}, v|||^2_{\boldsymbol{\Theta}} \geq C||v||^2_{H^1(\Omega)} \quad \forall \boldsymbol{\eta} \in \boldsymbol{\Theta}_0,\ v \in W_0 \ ,$$

with $C$ independent of $h$ and $t$. Therefore, the norm $|||\cdot|||_{\boldsymbol{\Theta}}$ also includes the $H^1$ norm of both rotations and deflections.

The following stability result can be shown adopting well-known techniques, cf. [6], combined with the results Section 4. Therefore, the proof will be only sketched and several details will be omitted.

**Proposition 5.1.** *For all* $(\boldsymbol{\beta}_h, u_h, \boldsymbol{\tau}_h) \in \boldsymbol{\Theta}_{0,h}, W_{0,h}, \boldsymbol{\Sigma}_{0,h}$*, there exists* $(\boldsymbol{\eta}_h, v_h, \boldsymbol{s}_h)) \in \boldsymbol{\Theta}_{0,h}, W_{0,h}, \boldsymbol{\Sigma}_{0,h}$ *such that*

$$\mathcal{B}(\boldsymbol{\beta}_h, u_h, \boldsymbol{\tau}_h; \boldsymbol{\eta}_h, v_h, \boldsymbol{s}_h) \geq C_1|||\boldsymbol{\beta}_h, u_h, \boldsymbol{\tau}_h|||^2 \ , \tag{30}$$

$$|||\boldsymbol{\eta}_h, v_h, \boldsymbol{s}_h||| \leq C_2|||\boldsymbol{\beta}_h, u_h, \boldsymbol{\tau}_h||| \ , \tag{31}$$

*with* $C_1$ *and* $C_2$ *positive constants independent of* $h$ *and* $t$*.*

*Proof.* Taking $(\boldsymbol{\eta}_h^1, v_h^1, \boldsymbol{s}_h^1) = (\boldsymbol{\beta}_h, u_h, -\boldsymbol{\tau}_h)$ in (19), one immediately gets

$$\mathcal{B}(\boldsymbol{\beta}_h, u_h, \boldsymbol{\tau}_h; \boldsymbol{\eta}_h^1, v_h^1, \boldsymbol{s}_h^1) \geq C||\boldsymbol{\beta}_h||^2_{H^1(\Omega)} + t^2||\boldsymbol{\tau}_h||^2_{L^2(\Omega)} \ , \tag{32}$$

$$|||\boldsymbol{\eta}_h^1, v_h^1, \boldsymbol{s}_h^1||| \leq |||\boldsymbol{\beta}_h, u_h, \boldsymbol{\tau}_h||| \ . \tag{33}$$

Due to (16), we can choose $(\boldsymbol{\eta}_h^2, v_h^2, \boldsymbol{s}_h^2) \in \boldsymbol{\Theta}_{0,h} \times W_{0,h} \times \boldsymbol{\Sigma}_{h,0}$ such that

$$\begin{aligned} &\boldsymbol{s}_h^2 = \boldsymbol{0} \\ &\boldsymbol{\eta}_h^2 - \nabla v_h^2 = h^2\boldsymbol{\tau}_h \\ &\|\boldsymbol{\eta}_h^2\|_{H^1(\Omega)} + \|v_h^2\|_{H^1(\Omega)} \leq Ch\|\boldsymbol{\tau}_h\|_{L^2(\Omega)} \ . \end{aligned} \tag{34}$$

The Cauchy-Schwarz inequality yields

$$\begin{aligned}\mathcal{B}(\boldsymbol{\beta}_h, u_h, \boldsymbol{\tau}_h; \boldsymbol{\eta}_h^2, v_h^2, \boldsymbol{s}_h^2) &= a(\boldsymbol{\beta}_h, \boldsymbol{\eta}_h^2) + h^2||\boldsymbol{\tau}_h||^2_{L^2(\Omega)} \\ &\geq h^2||\boldsymbol{\tau}_h||^2_{L^2(\Omega)} - C||\boldsymbol{\beta}_h||_{H^1(\Omega)}||\boldsymbol{\eta}_h^2||_{H^1(\Omega)} \\ &\geq h^2||\boldsymbol{\tau}_h||^2_{L^2(\Omega)} - Ch||\boldsymbol{\beta}_h||_{H^1(\Omega)}||\boldsymbol{\tau}_h^2||_{H^1(\Omega)} \ .\end{aligned} \tag{35}$$

Applying the arithmetic-geometric mean inequality, from (34)–(35) one easily gets

$$\mathcal{B}(\boldsymbol{\beta}_h, u_h, \boldsymbol{\tau}_h; \boldsymbol{\eta}_h^2, v_h^2, \boldsymbol{s}_h^2) \geq \frac{1}{2}h^2||\boldsymbol{\tau}_h||^2_{L^2(\Omega)} - C'||\boldsymbol{\beta}_h||^2_{H^1(\Omega)} \ . \tag{36}$$

Furthermore, by definition (29), recalling (7) and (34), one has

$$|||\boldsymbol{\eta}_h^2, v_h^2, \boldsymbol{s}_h^2||| \leq C\Big(h||\boldsymbol{\tau}||_{L^2(\Omega)} + \frac{h^2}{t+h}||\boldsymbol{\tau}||_{L^2(\Omega)}\Big) \leq C|||\boldsymbol{\beta}_h, u_h, \boldsymbol{\tau}_h||| \ . \tag{37}$$

We finally select $(\boldsymbol{\eta}_h^3, v_h^3, \boldsymbol{s}_h^3) = (0, 0, (t+h)^{-2}(\boldsymbol{\beta}_h - \nabla u_h))$. Using again the arithmetic-geometric mean inequality and some simple algebra, we obtain

$$\begin{aligned}\mathcal{B}(\boldsymbol{\beta}_h, u_h, \boldsymbol{\tau}_h; \boldsymbol{\eta}_h^3, v_h^3, \boldsymbol{s}_h^3) &= \frac{1}{(t+h)^2}||\boldsymbol{\beta}_h - \nabla u_h||^2_{L^2(\Omega)} - \frac{t^2}{(t+h)^2}(\boldsymbol{\tau}, \boldsymbol{\beta}_h - \nabla u_h) \\ &\geq \frac{1}{2(t+h)^2}||\boldsymbol{\beta}_h - \nabla u_h||^2_{L^2(\Omega)} - C\frac{t^4}{(t+h)^2}||\boldsymbol{\tau}_h||^2_{L^2(\Omega)} \\ &\geq \frac{1}{2(t^2+h^2)}||\boldsymbol{\beta}_h - \nabla u_h||^2_{L^2(\Omega)} - Ct^2||\boldsymbol{\tau}_h||^2_{L^2(\Omega)} \ .\end{aligned} \tag{38}$$

Moreover, recalling (29) and (7), it follows

$$|||\boldsymbol{\eta}_h^3, v_h^3, \boldsymbol{s}_h^3||| \leq C(t+h)^{-1}||\boldsymbol{\beta}_h - \nabla u_h||_{L^2(\Omega)} \leq C|||\boldsymbol{\beta}_h, u_h, \boldsymbol{\tau}_h||| \ . \tag{39}$$

We now consider the linear combination

$$(\boldsymbol{\eta}_h, v_h, \boldsymbol{s}_h) = \sum_{i=1}^{3} c_i(\boldsymbol{\eta}_h^i, v_h^i, \boldsymbol{s}_h^i) \ ,$$

with positive $c_i \in \mathbb{R}$. Estimates (30) and (31) follow from a suitable choice of the coefficients $c_i$, by using (32)–(33), (36)–(37) and (38)–(39).

□

From Proposition 5.1, the following result is easily deduced.

**Proposition 5.2.** *Let $(\boldsymbol{\theta}, w)$ be the solution of Problem (1) and $(\boldsymbol{\theta}_h, w_h)$ be the solution of Problem (17). Let the shears $\boldsymbol{\gamma} = t^{-2}(\boldsymbol{\theta} - \nabla w)$ and $\boldsymbol{\gamma}_h = t^{-2}(\boldsymbol{\theta}_h - \nabla w_h)$. Then, for any $(\boldsymbol{\theta}_I, w_I, \boldsymbol{\gamma}_I)$ in $\boldsymbol{\Theta}_{0,h} \times W_{0,h} \times \boldsymbol{\Sigma}_{0,h}$ it holds*

$$|||\boldsymbol{\theta} - \boldsymbol{\theta}_h, w - w_h, \boldsymbol{\gamma} - \boldsymbol{\gamma}_h||| \leq C|||\boldsymbol{\theta} - \boldsymbol{\theta}_I, w - w_I, \boldsymbol{\gamma} - \boldsymbol{\gamma}_I||| \ ,$$

*where the constant $C$ is independent of $h, t$.*

*Proof.* The proof is a consequence of standard consistency-stability arguments. We apply Proposition 5.1 to the difference $(\boldsymbol{\theta}_h - \boldsymbol{\theta}_I, w_h - w_I, \boldsymbol{\gamma}_h - \boldsymbol{\gamma}_I)$, then apply the error equation given by (20) and (21), to derive

$$|||\boldsymbol{\theta}_h - \boldsymbol{\theta}_I, w_h - w_I, \boldsymbol{\gamma}_h - \boldsymbol{\gamma}_I|||^2 \leq C\mathcal{B}(\boldsymbol{\theta} - \boldsymbol{\theta}_I, w - w_I, \boldsymbol{\gamma} - \boldsymbol{\gamma}_I; \boldsymbol{\eta}_h, v_h, \boldsymbol{s}_h) \ , \quad (40)$$

where

$$|||\boldsymbol{\eta}_h, v_h, \boldsymbol{s}_h||| \leq |||\boldsymbol{\theta}_h - \boldsymbol{\theta}_I, w_h - w_I, \boldsymbol{\gamma}_h - \boldsymbol{\gamma}_I||| \ . \quad (41)$$

Observing that the bilinear form $\mathcal{B}$ is bounded with respect to the norm $|||\cdot|||$ and applying (41), bound (40) gives

$$|||\boldsymbol{\theta}_h - \boldsymbol{\theta}_I, w_h - w_I, \boldsymbol{\gamma}_h - \boldsymbol{\gamma}_I||| \leq C|||\boldsymbol{\theta} - \boldsymbol{\theta}_I, w - w_I, \boldsymbol{\gamma} - \boldsymbol{\gamma}_I||| \ .$$

The result follows using the triangle inequality.

□

Combining the above proposition with the interpolation results of Lemma 4.3 the next Corollary easily follows.

**Corollary 5.1.** *Let $(\boldsymbol{\theta}, w)$ be the solution of Problem (1) and $(\boldsymbol{\theta}_h, w_h)$ be the solution of Problem (17). Let the shears $\boldsymbol{\gamma} = t^{-2}(\boldsymbol{\theta} - \nabla w)$ and $\boldsymbol{\gamma}_h = t^{-2}(\boldsymbol{\theta}_h - \nabla w_h)$. Then, provided the solution of (1) is sufficiently regular for the right-hand-side to make sense, for all $1 < s \leq p$ it holds*

$$|||\boldsymbol{\theta} - \boldsymbol{\theta}_h, w - w_h, \boldsymbol{\gamma} - \boldsymbol{\gamma}_h||| \leq Ch^{s-1}\Big(||\boldsymbol{\theta}||_s + ||w||_{s+1} + ||\boldsymbol{\gamma}||_{\max(0,s-2)} + t||\boldsymbol{\gamma}||_{s-1}\Big) \ ,$$

*where the constant $C$ is independent of $h$ and $t$.*

We note that the regularity required in Corollary 5.1 may be unrealistic for high values $s$, due to the presence of boundary layers (see for instance [31]).

*5.3. Improved convergence rates*

We start this section with the following lemma, which shows an improved convergence property for the $L^2$ norm of the rotations. We omit the proof, since it merely adopts a classical Aubin-Nietsche argument.

**Lemma 5.2.** *Let the Problem* (1) *be regular. Then, under the notation of Proposition 5.2, it holds*

$$||\boldsymbol{\theta} - \boldsymbol{\theta}_h||_{L^2(\Omega)} \leq Ch\Big(||\boldsymbol{\theta} - \boldsymbol{\theta}_h||_{H^1(\Omega)} + t||\boldsymbol{\gamma} - \boldsymbol{\gamma}_h||_{L^2(\Omega)}\Big)$$

*with $C$ independent of $h, t$.*

We remark that the regularity of Problem (1) holds, for instance, when the domain $\Omega$ is convex and the plate is clamped on the whole boundary [32]. For more general cases we refer the reader to [31, 32] where the (smooth) boundary layers and the effect of corners are respectively investigated.

The following result gives an improved convergence rate of convergence for the deflection variable.

**Lemma 5.3.** *Under the assumptions and notation of Lemma 5.2, for any interpolant $w_I \in W_{h,0}$, it holds*

$$||w - w_h||_{H^1(\Omega)} \leq Ch\Big(||\boldsymbol{\theta} - \boldsymbol{\theta}_h||_{H^1(\Omega)} + t||\boldsymbol{\gamma} - \boldsymbol{\gamma}_h||_{L^2(\Omega)}\Big) + ||\nabla(w - w_I)||_{L^2(\Omega)}$$

*with $C$ independent of $h$ and $t$.*

*Proof.* Testing Problems (1) and (17) with the choice $(\mathbf{0}, v_h) \in \boldsymbol{\Theta}_{h,0} \times W_{h,0}$, and taking the difference, one obtains

$$(\nabla(w - w_h), \nabla v_h) = (\boldsymbol{\theta} - \boldsymbol{\theta}_h, \nabla v_h) \ .$$

Thus, setting $v_h = w_h - w_I$ one gets

$$\begin{aligned} ||\nabla(w_h - w_I)||^2_{L^2(\Omega)} &= (\nabla(w_h - w_I), \nabla v_h) \\ &= (\nabla(w_h - w), \nabla v_h) + (\nabla(w - w_I), \nabla v_h) \\ &= (\boldsymbol{\theta} - \boldsymbol{\theta}_h, \nabla v_h) + (\nabla(w - w_I), \nabla v_h). \end{aligned} \tag{42}$$

Applying the Poincaré inequality, then using (42) and the Cauchy-Schwarz inequality, we obtain

$$||w_h - w_I||_{H^1(\Omega)} \leq C||\nabla(w_h - w_I)||_{L^2(\Omega)} \leq C||\boldsymbol{\theta} - \boldsymbol{\theta}_h||_{L^2(\Omega)} + ||\nabla(w - w_I)||_{L^2(\Omega)} \ .$$

The result trivially follows from the above bound, combined with the triangle inequality and Lemma 5.2.

□

Note that in the proposed method the approximation order of the space $W_h$ is one point higher with respect to the rotation space $\mathbf{\Theta}_h$, as shown in Lemma 4.3. Therefore, the above result indeed implies an improved rate of convergence with respect to Proposition 5.2.

## 6. Numerical tests

In this section we present some numerical experiments to show the actual performance of the numerical methods introduced in Section 4. For all tests, we select a material with Poisson's ratio $\nu = 0.3$ and Young's modulus $E = 1.092 \cdot 10^7 N/m^2$. Accordingly, we will always express forces and lengths in $N$ and $m$, respectively.

In all the tests we start from the mesh used for the geometry representation and we build the different components of the approximation spaces performing three simple steps:

1. degree elevation of the basis function used for the mapping, to the requested degree of the given field component;
2. knot repetitions in order to have the proper continuity;
3. the $h$-refinement is performed using uniform knot insertions in the original knots vectors.

We remark that, if the geometry is described by NURBS, step 1. is perfomed on the B-splines basis obtained by setting the NURBS weight to one.

### *6.1. Case 1: fully hardly clamped square plate.*

We consider a problem having a known the analytical solution (see [33]). This test consists of a unitary square block $[0,1]^2$ with all the four sides clamped, i.e., $\Gamma = \Gamma_c$, subject to a body load given by

$$\begin{aligned} f(x,y) = \frac{E}{12(1-\nu^2)} \big[ & 12y(y-1)(5x^2-5x+1)(2y^2(y-1)^2 \\ & + x(x-1)(5y^2-5y+1)) \\ & + 12x(x-1)(5y^2-5y+1)(2x^2(x-1)^2 \\ & + y(y-1)(5x^2-5x+1))\big] \ . \end{aligned}$$

The analytical solution is

$$\boldsymbol{\theta}(x,y) = \begin{pmatrix} y^3(y-1)^3x^2(x-1)^2(2x-1) \\ \\ x^3(x-1)^3y^2(y-1)^2(2y-1) \end{pmatrix}$$

$$\begin{aligned} w(x,y) = \frac{1}{3}x^3(x-1)^3y^3(y-1)^3 \\ - \frac{2t^2}{5(1-\nu)}\big[y^3(y-1)^3x(x-1)(5x^2-5x+1) \\ + x^3(x-1)^3y(y-1)(5y^2-5y+1)\big] \, . \end{aligned}$$

In Figure 1 we plot the $H^1$-norm approximation error for the displacement field $w(x,y)$ and for the rotation field $\boldsymbol{\theta}(x,y)$. We run tests with $p = 3,\ 4$ ad $\alpha = 2,\ 3$ both for deflections and rotations, respectively, and the thickness $t = 10^{-3}$. Figure 1 clearly displays convergence rates in perfect agreement with the theoretical results of Section 5.

In addition, we performed simulations (not reported here) using also $t \in \{10^{-1}, 10^{-2}, 10^{-4}\}$, and we found that the methods are substantially insensitive to thickness changes.

*6.2. Case 2: quarter of an annulus with four hardly simply supported sides.*

The second test consists in a fully hardly simply supported quarter of an annulus plate., i.e., $\Gamma = \Gamma_{sh}$ (see Figure 2) and loaded by

$$f(x,y) = 10^4 \ \sin\big(2\arctan(\tfrac{y}{x})\big) \, .$$

In this case the analytical solution is not available. Therefore, we use as reference solution the one computed on a fine mesh ($h = 1/256$) and with degree $p = 3$ and regularity index $\alpha = 2$ both for deflections and rotations. The same degree and regularity index are used for the simulations on the coarser meshes.

In Figure 3 and Figure 4 we plot the $H^1$-norm approximation errors for $t = 10^{-2}$ and $t = 10^{-3}$ respectively. Once again, an excellent agreement with the theoretical predictions can be noticed.

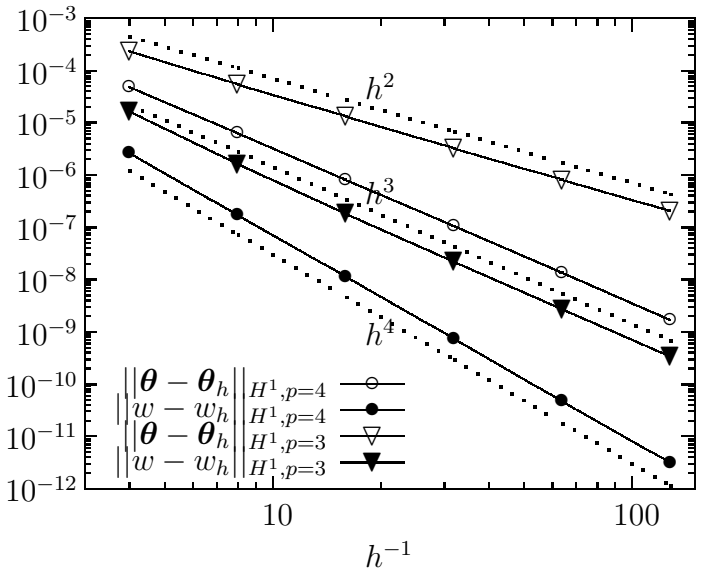


Figure 1: Case 1 (square with four sides hardly clamped), $t = 10^{-3}$.

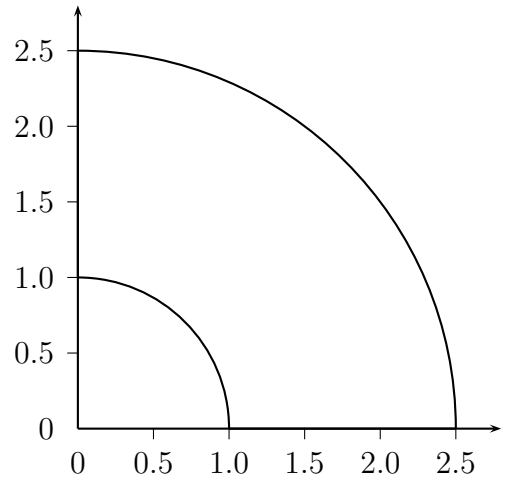


Figure 2: Fully hardly simply supported annular plate.

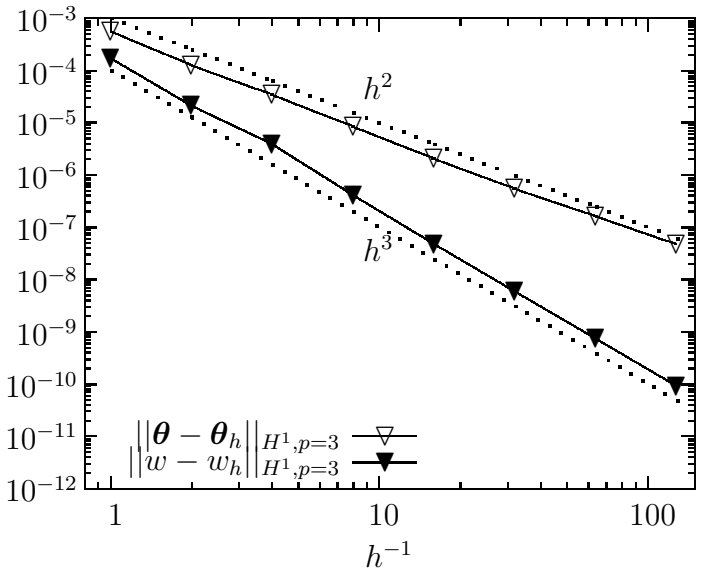


Figure 3: Case 2 (fully hardly simply supported annular plate). $p = 3$, $t = 10^{-2}$.

*6.3. Case 3: boundary layer test problem*

The third test problem shares the same load and geometry used for Case 2 (Figure 2), but with different boundary conditions. More precisely, we set $\Gamma_c = \emptyset$ and

- $\Gamma_{ss} = \{(x, y) \in \mathbb{R}^2 \ : \ x^2 + y^2 = 1\}$;
- $\Gamma_{sh} = \{(0, y) \ : \ 1 < y < 2.5\} \cup \{(x, 0) \ : \ 1 < x < 2.5\}$
- $\Gamma_f = \{(x, y) \in \mathbb{R}^2 \ : \ x^2 + y^2 = \frac{25}{4}\}$.

On the curved parts of the boundary, this problem exhibits a boundary layer whose characteristic length is $O(t)$ (see [31]). In our computations we set $t = 10^{-2}$, and $p = 3$, $\alpha = 2$ both for deflections and rotations. For this test case we always plot, in log-log scale, the errors versus $N_{DOF}^{1/2}$, where $N_{DOF}$ denotes the total number of degrees of freedom. We remark that for uniform meshes, $N_{DOF}^{1/2}$ behaves like $h^{-1}$.

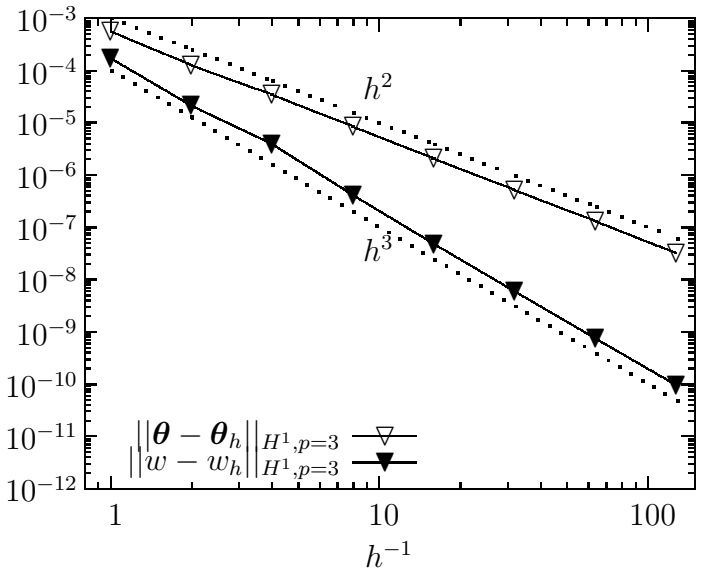


Figure 4: Case 2 (fully hardly simply supported annular plate). $p = 3$, $t = 10^{-3}$.

As for Case 2, the analytical solution is not available, and a reference numerical solution is obtained using a very fine mesh.

Figure 6 displays the error behaviour when using a uniform mesh refinement. It is worth noticing that a severe suboptimal convergence rate occurs as long as the mesh is not sufficiently fine to resolve the boundary layer. Of course, this phenomenon implies that uniform meshes requires an excessive number of degrees of freedom to significantly reduce the error, especially for small plate thicknesses.

We now employ a sequence of meshes adapted to the boundary layers (Figure 5), using the following procedure. An initial mesh consisting of three elements is set up as in Figure 5. The width of both the layer elements is 0.045 (corresponding to 3% of the total annulus width). The finer meshes are then obtained by uniform refinement of each of the three initial elements. Figure 7 shows the error behaviour using that mesh sequence. We notice

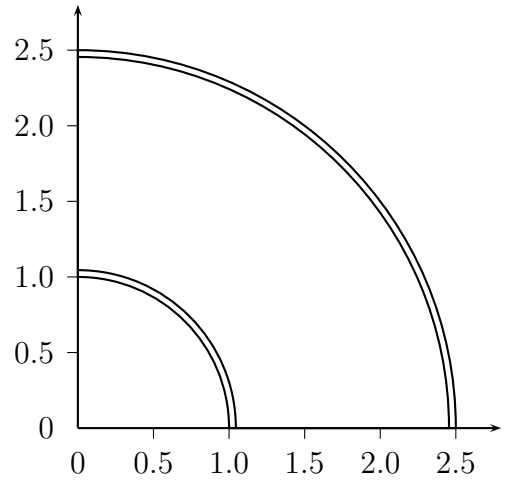


Figure 5: Coarsest mesh for the layers-adapted case.

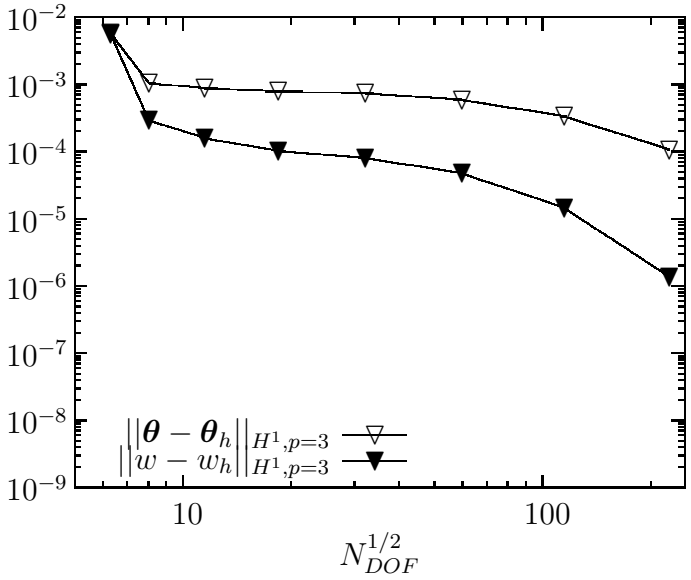


Figure 6: Case 3 (quarter of ring with boundary layers). Uniform mesh. $p = 3$, $t = 10^{-2}$

that the optimal convergence rate for the $H^1$-norm error is now restored.

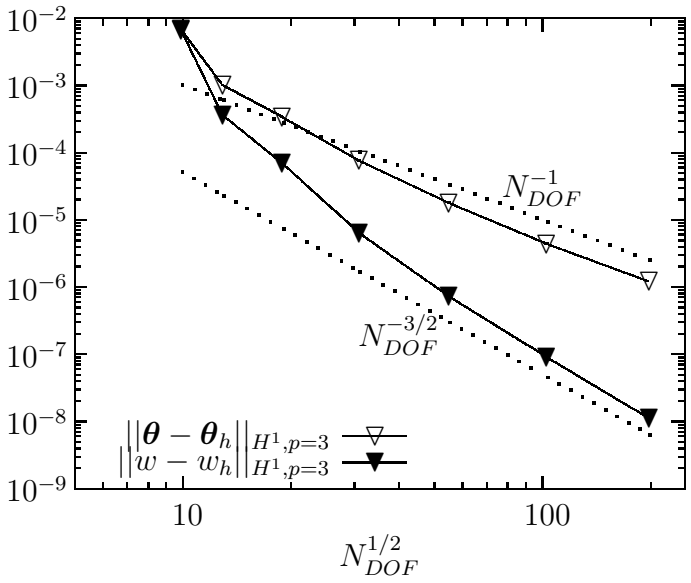


Figure 7: Case 3 (quarter of ring with boundary layers). Layers-adapted mesh. $p = 3$, $t = 10^{-2}$.


## Acknowledgments

The authors were partially supported by the European Research Council through the FP7 Ideas Starting Grant 205004: *GeoPDEs - Innovative compatible discretization techniques for partial differential equations*, and by the Italian MIUR through the FIRB "Futuro in Ricerca" Grant RBFR08CZ0S *Discretizzazioni Isogeometriche per la Meccanica del Continuo*. Giancarlo Sangalli was also partially supported by the European Research Council Ideas Starting Grant 259229: *ISOBIO - Isogeometric Methods for Biomechanics*. This support is gratefully acknowledged.

## References


[1] F. Brezzi, M. Fortin, Mixed and Hybrid Finite Element Methods, Springer, New York, 1991.

[2] D. N. Arnold, R. S. Falk, A uniformly accurate finite element method for the Reissner-Mindlin plate, SIAM J. Numer. Anal. 26 (1989) 1276–1290.

[3] F. Auricchio, C. Lovadina, Analysis of kinematic linked interpolation methods for Reissner-Mindlin plate problems, Comput. Methods Appl. Mech. Engrg. 190 (2001) 2465–2482.

[4] L. Beirão da Veiga, Finite element methods for a modified Reissner-Mindlin free plate model, SIAM J. Numer. Anal. 42 (2004) 1572–1591.

[5] F. Brezzi, M. Fortin, R. Stenberg, Error analysis of mixed-interpolated elements for Reissner-Mindlin plates, Math. Models Meth. Appl. Sci. 1 (1991) 125–151.

[6] D. Chapelle, R. Stenberg, An optimal low-order locking-free finite element method for Reissner-Mindlin plates, Math. Models Methods Appl. Sci. 8 (1998) 407–430.

[7] R. Duran, E. Liberman, On mixed finite element methods for the Reissner-Mindlin plate model, Math. Comp. 58 (1992) 561–573.

[8] R. S. Falk, T. Tu, Locking-free finite elements for the Reissner-Mindlin plate, Math. Comp. 69 (2000) 911–928.

[9] T. J. R. Hughes, L. P. Franca, A mixed finite element formulation for Reissner-Mindlin plate theory: uniform convergence of all higher-order spaces, Comput. Methods Appl. Mech. Engrg. 67 (1988) 223–240.

[10] C. Lovadina, A low-order nonconforming finite element for Reissner-Mindlin plates, SIAM J. Numer. Anal. 42 (2005) 2688–2705.

[11] C. Lovadina, Analysis of a mixed finite element method for the Reissner-Mindlin plate problems, Comput. Methods Appl. Mech. Engrg. 163 (1998) 71–85.

[12] A. Tessler, T. J. R. Hughes, A three-node Mindlin plate element with improved transverse shear, Comput. Methods Appl. Mech. Engrg. 50 (1985) 1–101.

[13] T. J. R. Hughes, J. A. Cottrell, Y. Bazilevs, Isogeometric analysis: CAD, finite elements, NURBS, exact geometry and mesh refinement, Comput. Methods Appl. Mech. Engrg. 194 (2005) 4135–4195.

[14] Y. Bazilevs, V. M. Calo, T. J. R. Hughes, Y. Zhang, Isogeometric fluid-structure interaction: theory, algorithms, and computations, Comput. Mech. 43 (2008) 3–37.

[15] A. Buffa, C. de Falco, G. Sangalli, Isogeometric Analysis: new stable elements for the Stokes equation, 2010. To appear on Inter. J. Numer. Meth. Fluids. DOI: 10.1002/fld.2337.

[16] F. Auricchio, L. Beirão da Veiga, C. Lovadina, A. Reali, The importance of the exact satisfaction of the incompressibility constraint in nonlinear elasticity: mixed FEMs versus NURBS-based approximations, Comput. Methods Appl. Mech. Engrg. (199) 314–323.

[17] F. Auricchio, L. Beirão da Veiga, A. Buffa, C. Lovadina, A. Reali, G. Sangalli, A fully "locking-free" isogeometric approach for plane linear elasticity problems: a stream function formulation, Comput. Methods Appl. Mech. Engrg. 197 (2007) 160–172.

[18] D. J. Benson, Y. Bazilevs, M. C. Hsu, T. J. R. Hughes, Isogeometric shell analysis: The Reissner-Mindlin shell, Comput. Methods Appl. Mech. Engrg. 199 (2010) 276–289.

[19] S. Lipton, J. A. Evans, Y. Bazilevs, T. Elguedj, T. J. R. Hughes, Robustness of isogeometric structural discretizations under severe mesh distortion, Comput. Methods Appl. Mech. Engrg. 199 (2010) 353–373.

[20] A. Buffa, G. Sangalli, R. Vázquez, Isogeometric analysis in electromagnetics: B-splines approximation, Comput. Methods Appl. Mech. Engrg. 199 (2010) 1143–1152.

[21] A. Buffa, J. Rivas, G. Sangalli, R. Vázquez, Isogeometric Discrete Differential Forms in Three Dimensions, 2011. To appear on SIAM J. Numer. Anal. DOI: 10.1137/100786708.

[22] J. A. Cottrell, T. J. R. Hughes, Y. Bazilevs, Isogeometric Analysis. Towards integration of CAD and FEA, Wiley, 2009.

[23] T. J. R. Hughes, A. Reali, G. Sangalli, Duality and Unified Analysis of Discrete Approximations in Structural Dynamics and Wave Propagation: Comparison of $p$-method Finite Elements with $k$-method NURBS, Comput. Methods Appl. Mech. Engrg. 197 (2008) 4104–4124.

[24] L. Beirão da Veiga, A. Buffa, J. Rivas, G. Sangalli, Some estimates for $h-p-k-$refinement in isogeometric analysis, 2010. To appear on Numer. Math. DOI: 10.1007/s00211-010-0338-z.

[25] J. A. Evans, Y. Bazilevs, I. Babuška, T. J. R. Hughes, $n$-width, sup-infs, and optimality ratios for the $k$-version of the isogeometric finite element method, Comput. Methods Appl. Mech. Engrg. 198 (2009) 1726–1741.

[26] D. N. Arnold, R. S. Falk, R. Winther, Finite element exterior calculus: from Hodge theory to numerical stability, Bull. Amer. Math. Soc. (N.S.) 47 (2010) 281–354.

[27] I. Babuska, J. Pitkäranta, The plate paradox for hard and soft simple support, Technical Report, Inst. for Phys. Sci. and Tech., Univ. of Maryland, 1988.

[28] C. de Boor, A practical guide to splines, volume 27 of *Applied Mathematical Sciences*, Springer-Verlag, New York, revised ed. edition, 2001.

[29] Y. Bazilevs, L. Beirão da Veiga, J. A. Cottrell, T. J. R. Hughes, G. Sangalli, Isogeometric analysis: approximation, stability and error estimates for $h$-refined meshes, Math. Models Methods Appl. Sci. 16 (2006) 1031–1090.

[30] F. Brezzi, K. J. Bathe, M. Fortin, Mixed-interpolated elements for Reissner-Mindlin plates, Inter. J. Numer. Methods Engrg. 28 (1989) 1787–1801.

[31] D. N. Arnold, R. S. Falk, Asymptotic analysis of the boundary layer for the Reissner-Mindlin plate model, SIAM J. Math. Anal. 27 (1996) 486–514.

[32] A. Rössle, A. M. Sändig, Corner singularities and regularity results for the Reissner/Mindlin plate model, J. of Elast. 103 (2011) 113–135.

[33] C. Chinosi, C. Lovadina, Numerical analysis of some mixed finite element methods for Reissner-Mindlin plates, Comput. Mech. 16 (1995) 36–44.